

Article

Microstructure and Magnetic Properties of M-Type $\text{Sr}_{0.1}\text{Ca}_{0.4}\text{La}_{0.5}\text{Fe}_{12}\text{O}_{19}$ Ferrites: The Impact of Different Precursors

Xiubin Zhao¹, Shuang Zhang¹, Jinsong Li¹, Ailin Xia^{1,*} and Yujie Yang² 

¹ School of Materials Science and Engineering, Anhui University of Technology, Maanshan 243002, China; xiubinzhao@163.com (X.Z.); 18325515939@163.com (S.Z.); ljs1176@126.com (J.L.)

² School of Materials Science and Engineering, Anhui University, Hefei 230601, China; loyalty-yyj@163.com

* Correspondence: alxia@ahut.edu.cn

Abstract: M-type $\text{Sr}_{0.1}\text{Ca}_{0.4}\text{La}_{0.5}\text{Fe}_{12}\text{O}_{19}$ powder specimens doped with different precursors RFe_2O_4 (R = Co, Ni, Cu, Zn, and Mg) were prepared via a traditional solid-state reaction method. The structural and magnetic properties of the specimens were studied. Only the single magnetoplumbite phase was found in all the specimens with uniformly distributed particles. The specimen with Zn-type precursor has the highest saturation (M_s), while the specimen with Co-type precursor has the highest remanent magnetism (M_r), coercivity (H_c), and the best comprehensive magnetic properties.

Keywords: M-type ferrites; solid state reaction; precursor; magnetic properties



Citation: Zhao, X.; Zhang, S.; Li, J.; Xia, A.; Yang, Y. Microstructure and Magnetic Properties of M-Type $\text{Sr}_{0.1}\text{Ca}_{0.4}\text{La}_{0.5}\text{Fe}_{12}\text{O}_{19}$ Ferrites: The Impact of Different Precursors. *Magnetochemistry* **2022**, *8*, 68. <https://doi.org/10.3390/magnetochemistry8070068>

Academic Editor: Jeremy M. Rawson

Received: 14 May 2022

Accepted: 24 June 2022

Published: 25 June 2022

Publisher's Note: MDPI stays neutral with regard to jurisdictional claims in published maps and institutional affiliations.



Copyright: © 2022 by the authors. Licensee MDPI, Basel, Switzerland. This article is an open access article distributed under the terms and conditions of the Creative Commons Attribution (CC BY) license (<https://creativecommons.org/licenses/by/4.0/>).

1. Introduction

M-type permanent magnetic ferrite is made from SrCO_3 , BaCO_3 or CaCO_3 and Fe_2O_3 as raw materials via a traditional ceramic process. It is a magnetic material of hexagonal magnetoplumbite structure, with high saturation magnetization (M_s), coercivity (H_c), and magnetic crystal anisotropy constant. It is mainly used in computer, office equipment, automotive, consumer electronics, aerospace, inductor, and electrical equipment industries [1,2]. In order to meet the various applications, many attempts have been made to improve the magnetic properties of M-type strontium ferrites by adding or doping some elements, such as La-Co, La-Ni, La-Zn, La-Cu, La-Mg, and other co-substitution of M-type ferrites [3–8]. L. Peng et al. [3] prepared La-Ni substituted M-type strontium ferrite by a microwave sintering method combined with a low-temperature sintering technology and studied the effect of La-Ni substitution amount on the magnetic properties of M-type strontium ferrite. When the La-Ni substitution amount was $x = 0.2$ ($\text{Sr}_{1-x}\text{La}_x\text{Fe}_{12-x}\text{Ni}_x\text{O}_{19}$), the material shows high anisotropic field H_a and coercivity H_c . Y. Ogata et al. [4] conducted a comparative study on the magnetic properties of M-type barium ferrite replaced by Cr^{3+} and La-Co, and the results showed that La-Co substitution could significantly improve the remanent magnetism (M_r) and the coercivity (H_c) at the same time. Y. J. Yang et al. [5] studied the influence of La-Cu substitution on the magnetic properties of M-type Barium/strontium ferrite, and the results showed that the M_r of specimens would increase first and then decrease with the increase in La-Cu substitution. L.S. You et al. [6] prepared M-type strontium ferrite substituted by La-Zn via a self-propagating high-temperature synthesis method, and it was found that La-Zn substitution significantly improved the magnetic properties of M-type strontium ferrite. In our previous study, the performance of ferrite could be significantly improved by the exchange coupling between the soft and hard magnetic phases. However, the influence of precursor addition on the structure and magnetic properties of M-type strontium calcium ferrites is still not reported. This research may help to replace rare earth elements with non-rare earth elements and thus reduce production costs.

In this study, the M-type $\text{Sr}_{0.1}\text{Ca}_{0.4}\text{La}_{0.5}\text{Fe}_{12}\text{O}_{19}$ magnetic powders with different precursors RFe_2O_4 (Co-, Ni-, Cu-, Zn-, and Mg-type) were prepared via a solid-state reaction method. The impact of different precursors on the structure and the magnetic properties of M-type strontium calcium ferrites $\text{Sr}_{0.1}\text{Ca}_{0.4}\text{La}_{0.5}\text{Fe}_{12}\text{O}_{19}$ are studied.

2. Experimental Procedure

2.1. RFe_2O_4 (R = Co, Ni, Cu, Zn and Mg) Precursors Preparation

The raw materials used in this study were analytically pure grade CuO, MgO, ZnO, Ni_2O_3 , Fe_2O_3 , and Co_2O_3 . Here, the preparation of the CoFe_2O_4 precursor is taken as the typical example. The mixed powders (Fe_2O_3 and Co_2O_3) were ball-milled in water for 2 h, and then the as-milled powders were dried at 850 °C in a muffle for 3 h in air. Finally, the calcined samples were pulverized to powders with a size smaller than 100 μm using a vibration mill for use as the Co-type precursor. Similarly, Ni-, Cu-, Zn-, and Mg-type precursors were also obtained according to the above steps, respectively.

2.2. Preparation of M-type Strontium Calcium Ferrite $\text{Sr}_{0.1}\text{Ca}_{0.4}\text{La}_{0.5}\text{Fe}_{12}\text{O}_{19}$ Powders with Different Precursors

All samples of M-type $\text{Sr}_{0.1}\text{Ca}_{0.4}\text{La}_{0.5}\text{Fe}_{12}\text{O}_{19}$ powders with different precursors (Co-, Ni-, Cu-, Zn-, and Mg-type) were prepared via a solid-state reaction method. The starting materials were SrCO_3 (98% purity), CaCO_3 (99% purity), La_2O_3 (99% purity), and Fe_2O_3 (98% purity). The mixed powders were placed in a sander containing hard alloy steel balls with a diameter of 6mm. The powders were milled in water for 2 h with an angular velocity of 400 rpm and a ball-to-powder weight ratio of 15:1, together with different RFe_2O_4 precursors of 3 wt%. Then, the as-milled powders were dried, pressed into pellets and calcined at a temperature of 1300 °C in a muffle for 2 h in air. Finally, the calcined samples were pulverized into powders to a size smaller than 100 μm using a vibration mill.

2.3. Characterization

The phase composition of the samples was identified by an X-ray diffractometer (XRD, PANalytical X'Pert Pro, Almelo, Netherlands) using $\text{Cu } K_{\alpha}$ ($\lambda = 1.5406 \text{ \AA}$) radiation. The morphologies of specimens were investigated using a field emission scanning electron microscope (FESEM, HITACHI S-4800, Tokyo, Japan). The room temperature (RT) magnetic hysteresis loops were measured on a vibrating sample magnetometer (VSM, MicroSense EZ7, Lowell, MA, USA) with a maximum external field of 20,000 Oe.

3. Results and Discussion

3.1. Structural Properties

Figure 1 displays the XRD patterns for $\text{Sr}_{0.1}\text{Ca}_{0.4}\text{La}_{0.5}\text{Fe}_{12}\text{O}_{19}$ powders with different precursors (Co-, Ni-, Cu-, Zn-, and Mg-type). As is shown, there is only the typical peak information from the magnetoplumbite phase found in this figure, which means that different precursor ions can enter the magnetoplumbite ferrite lattices without forming the second phases. However, the relative intensity of the diffraction peaks varies with the type of precursors. The strongest (008) peak was from the specimen with a Zn-type precursor, and the strongest peaks for the specimen with a Cu-type precursor were the (107) and (114) peaks. This indicates that they have different effects on the growth of each crystal plane with different precursors.

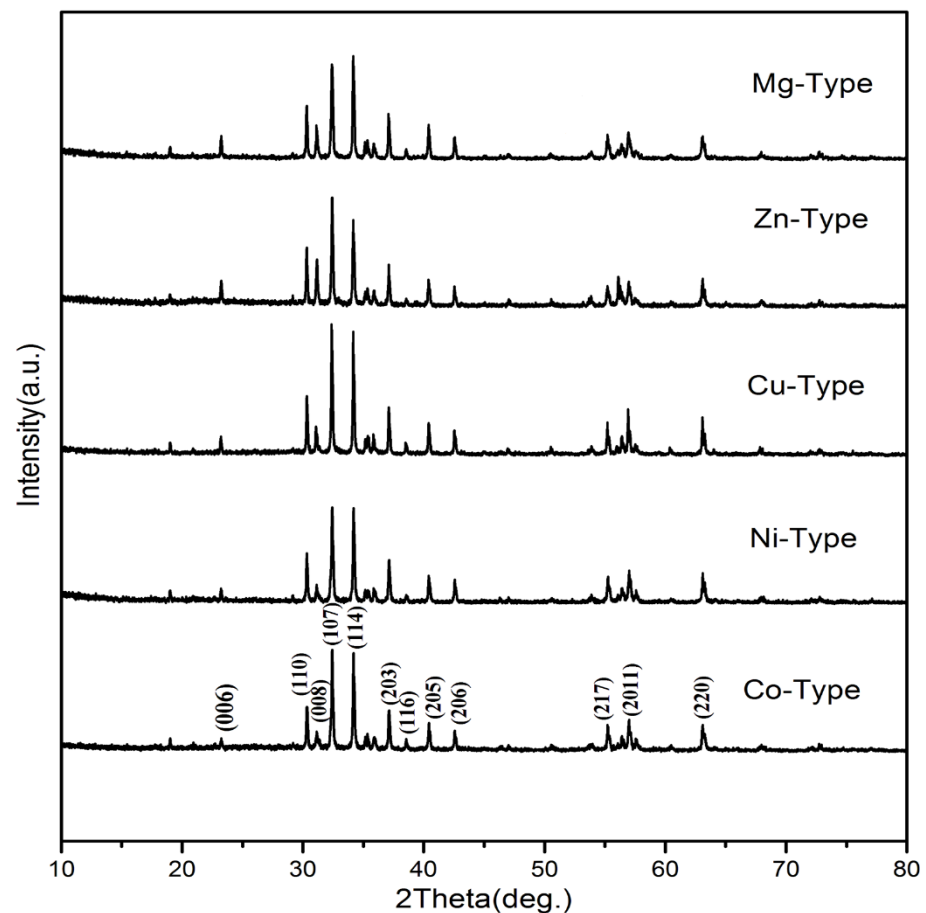


Figure 1. XRD patterns for $\text{Sr}_{0.1}\text{Ca}_{0.4}\text{La}_{0.5}\text{Fe}_{12}\text{O}_{19}$ powders with different precursors.

The lattice constants a and c were calculated using Miller indices (h , k , and l) and the inter-planer spacing d_{hkl} of (107) and (114) crystal planes according to the following Formula (1):

$$d_{hkl} = \left(\frac{4}{3} \cdot \frac{h^2 + hk + k^2}{a^2} + \frac{l^2}{c^2} \right)^{-1/2} \quad (1)$$

The change of lattice constants (a and c) and the crystal axis ratio of c/a of specimens with different precursors are shown in Figure 2. It can be seen that the lattice constant c of the specimens with Cu-type precursors had a maximum value of 22.9878 Å. However, for the specimen with Co-type precursors, the lattice constant (c) had a minimum value of 22.9624 Å.

From the inset of Figure 2, it can be observed that the crystal axis ratio of c/a is almost the same. According to the opinion of Versteegen and Stevels, the value of the c/a ratio presents the structure type [9]. The c/a is considered to be smaller than 3.98 for the SrM ferrites. The c/a ratios for the specimens with different precursors in this study ranged from 3.8952 to 3.9009, which are in good accord with the expected value of the M-type structure.

Figure 3 displays the density (ρ) of the specimens with different precursors. It can be seen from Figure 3 that the specimen with a Zn-type precursor has a maximum value of ρ (4.8570 g/cm³), while the specimen with an Mg-type precursor has a minimum value of ρ (4.1672 g/cm³).

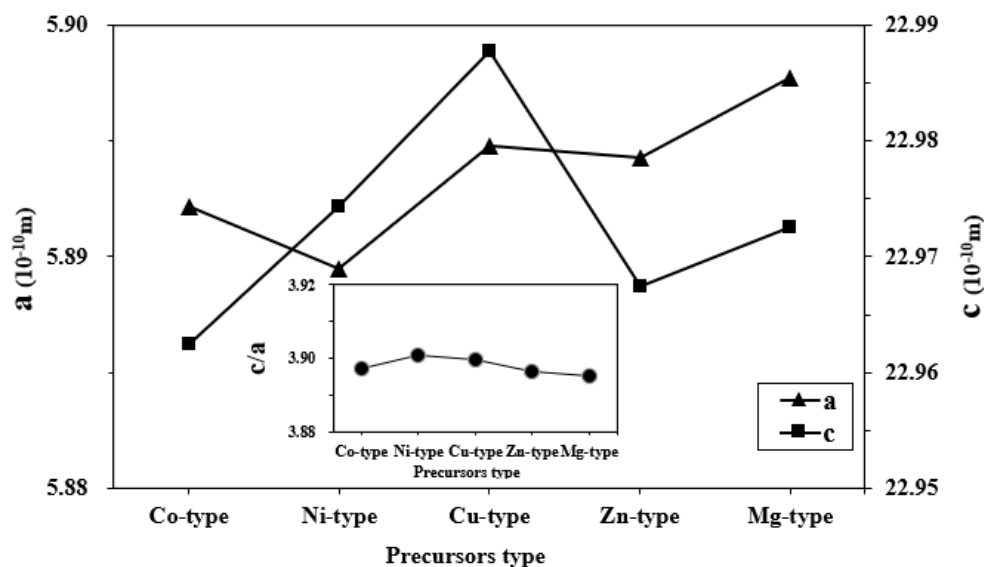


Figure 2. Lattice constants (a) and (c) of the specimens with different precursors; inset shows the crystal axis ratio of c/a of the specimen with different precursors.

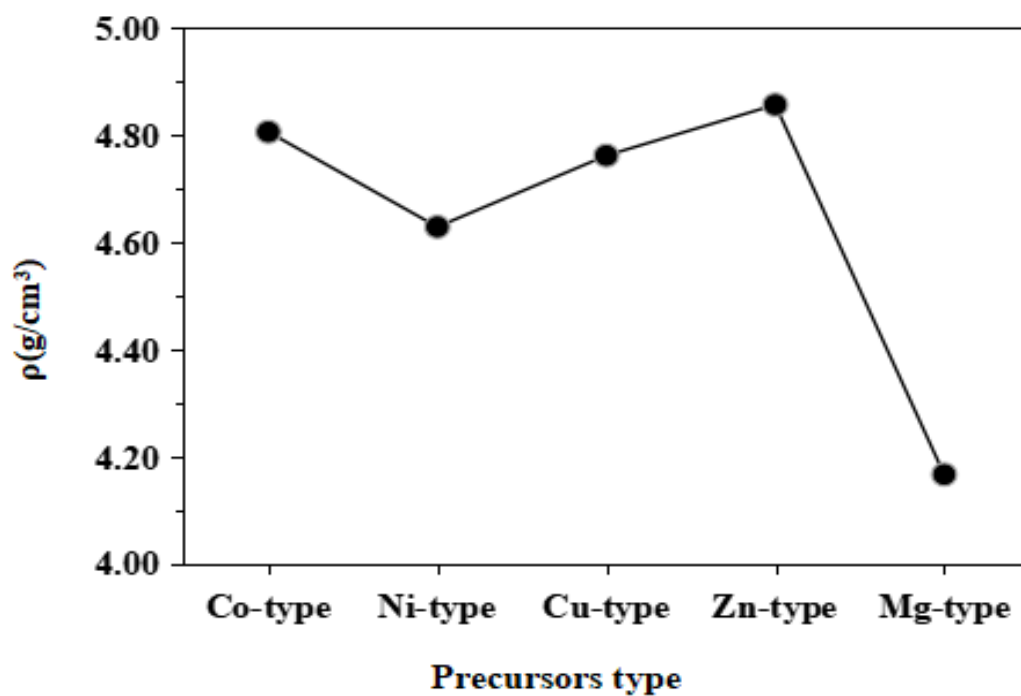


Figure 3. Density (ρ) of $\text{Sr}_{0.1}\text{Ca}_{0.4}\text{La}_{0.5}\text{Fe}_{12}\text{O}_{19}$ specimens with different precursors.

Figure 4 shows the typical FESEM images of the specimens. The grain size distribution of the specimens is shown in the upper right corner of the micrographs. As is shown in this figure, all the specimens with different precursors have formed the hexagonal structure, and the particles are distributed uniformly in size. In addition, the average particle size of specimens nearly remains unchanged for different precursors.

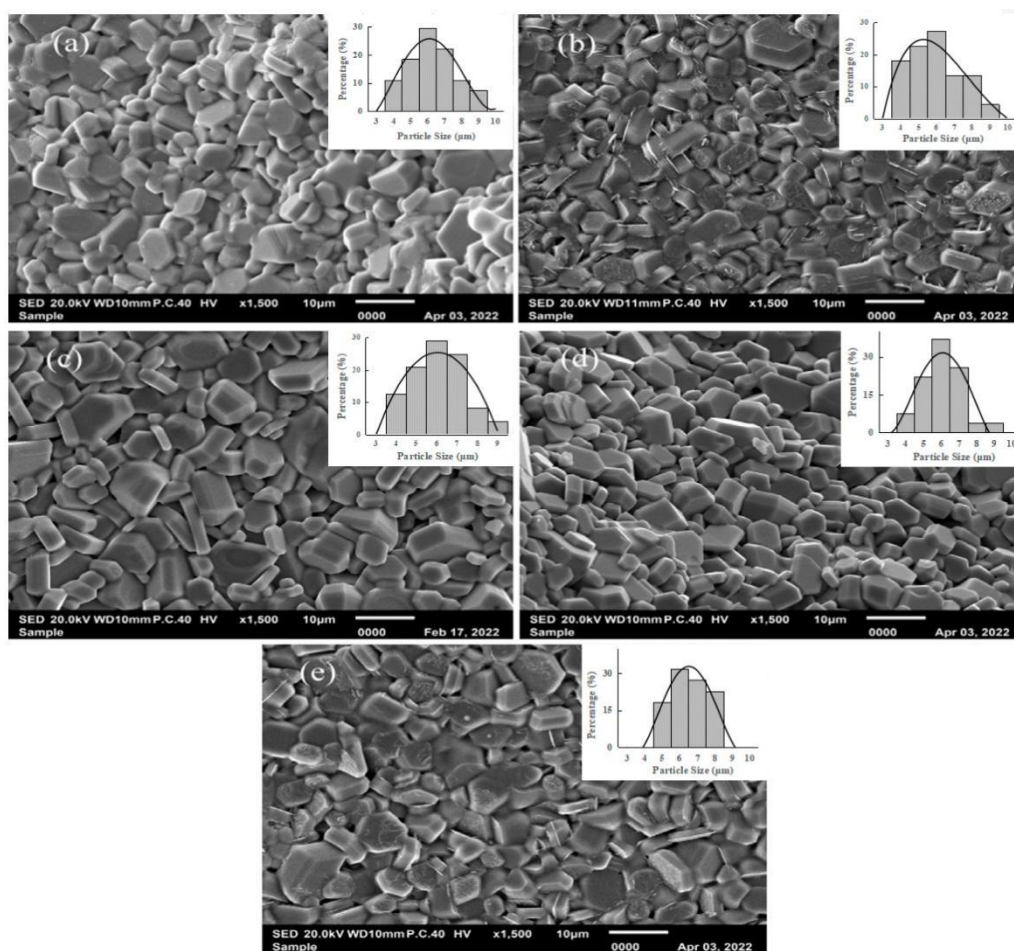


Figure 4. Typical SEM images of $\text{Sr}_{0.1}\text{Ca}_{0.4}\text{La}_{0.5}\text{Fe}_{12}\text{O}_{19}$ specimens with different precursors: (a) Co-, (b) Ni-, (c) Cu-, (d) Zn-, and (e) Mg-type.

3.2. Magnetic Properties

Figure 5 shows the RT magnetic hysteresis loops of the specimens with different precursors. The M_s , H_c , and remanent magnetization (M_r) of specimens with different precursors were obtained from Figure 5 and are listed in Table 1. As can be seen, the specimen with Zn-type precursor has the largest M_s (67.18 emu/g) but the smallest M_r (12.52 emu/g) and H_c (267 Oe). The specimens with Co-type precursors have the highest M_r and H_c together with the best comprehensive magnetic properties. However, the M_s , the M_r and the H_c of specimens are lower than those reported by Hessian et al. [10] and Rashad et al. [11].

Table 1. Magnetic properties of specimens with different precursors.

Precursors Type	M_s (emu/g)	M_r (emu/g)	H_c (Oe)
Co-type	66.20	31.83	1270
Ni-type	58.04	23.05	806
Cu-type	65.19	23.00	503
Zn-type	67.18	12.52	267
Mg-type	55.63	13.76	488

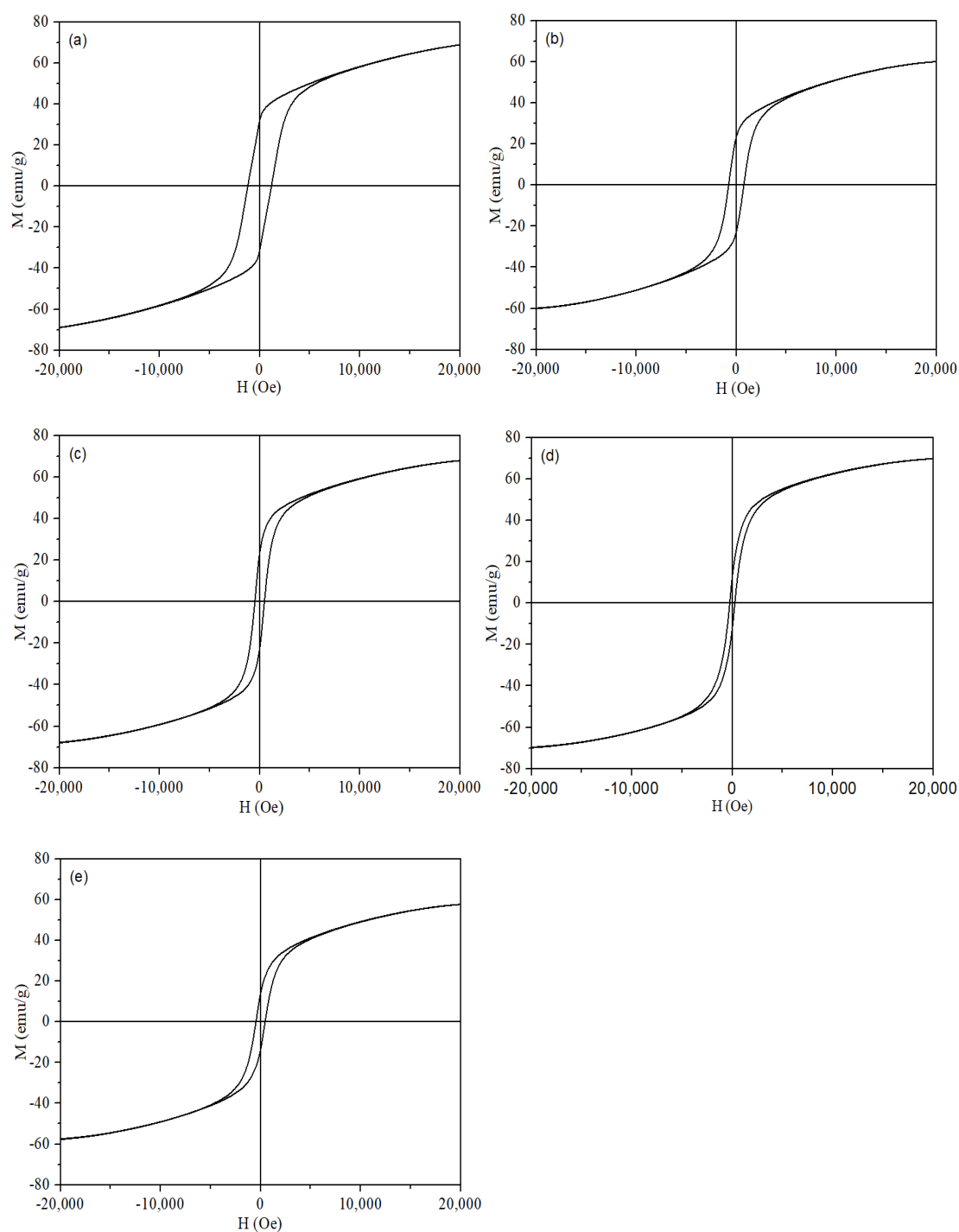


Figure 5. RT magnetic hysteresis loops of specimens with different precursors: (a) Co-, (b) Ni-, (c) Cu-, (d) Zn- and (e) Mg-type.

Within the basic M-type hexaferrite crystal structure, Fe^{3+} ions occupy five different sites, including spin-up sites ($2a$, octahedral sites; $2b$, trigonal bipyramid site; $12k$, octahedral sites) and spin-down sites ($4f_1$, tetrahedral site; $4f_2$, octahedral sites). The magnetic moment of the Fe^{3+} ion is $5 \mu_B$, and the molar ratio of Fe^{3+} ion at different lattice positions is $\text{Fe}(12k):\text{Fe}(2a):\text{Fe}(2b):\text{Fe}(4f_1):\text{Fe}(4f_2) = 6:1:1:2:2$. The total magnetic moment according to the molar ratio calculated is $20 \mu_B$, which determines the main factor of high saturation magnetization of the materials. At the same time, for different precursors, the difference of M_s mainly resulted from the influence of precursors on grain size, uniformity, and density of materials. It can be seen from Figure 4 that the particle distribution of specimens

is uniform, and the average particle size of specimens remains unchanged for different precursors. Therefore, the M_s is mainly affected by density, which results in the same variation tendency as density, shown in Figure 3. Due to the hexagonal structure and the lattice point occupied by Fe^{3+} ions, the SrM ferrite has high magnetocrystalline anisotropy. For ion substitutions, replacing Fe^{3+} ions will affect the magnetocrystalline anisotropy field for SrM ferrites and then leads to the change of H_c . The study of Mössbauer spectra of La–Co-substituted SrM ferrites revealed that most of the Co^{2+} ions were substituted for Fe^{3+} ions in $4f_2$ (mainly) and $2a$ octahedral sites [12–14]. The La^{3+} ions replaced most of the Sr^{2+} ions. Lechevallier et al. [15] reported that in the M-type ferrite phase, the presence of Co^{2+} ions could improve the solid solubility of rare-earth ions. E. Roohani et al. [16] reported that Ni^{2+} replaced the Fe^{3+} in $4f_2$ and $2b$ sites, resulting in the changes in the magnetocrystalline anisotropy constant. J.M. Bai et al. [17] reported that for the large substitution amount of La–Zn, the substitution of Fe^{3+} ions by Zn^{2+} ions could lead to the weakening of the strength of superexchange, which will lead to the transformation of the colinear arrangement of Fe^{3+} ions to the non-colinear arrangement, accompanied by the spin-inclined structure. L. Qiao et al. [18] reported that Cu^{2+} ions might preferentially replace Fe^{3+} ions at the spin-down $4f_2$ position. This occupation will increase the number of Fe^{3+} ions compared to the spin-down position, resulting in an enhanced Fe^{3+} –O– Fe^{3+} super exchange at $12k$ and $2b$ positions. Y.J. Yang et al. [19] reported that Mg^{2+} have a preference replaced the Fe^{3+} in $4f_1$ and $2a$ sites, which is ineffective in the reduction in the magnetocrystalline anisotropy. Therefore, the different H_c of specimens with different precursors in this study could be ascribed to the different degrees of influence on the magneto-crystalline anisotropic field.

4. Conclusions

The M-type strontium calcium ferrite $\text{Sr}_{0.1}\text{Ca}_{0.4}\text{La}_{0.5}\text{Fe}_{12}\text{O}_{19}$ specimens with different precursors were prepared via a solid-state reaction method. The effects of different precursors (Co-, Ni-, Cu-, Zn-, and Mg-type) on the structural and magnetic properties have been studied. The single magnetoplumbite phase was obtained in all the specimens. The SEM study showed that the particles were distributed uniformly in size. For the Zn-type precursor, the specimen has the highest saturation magnetization (M_s) but the lowest remanent magnetization (M_r) and coercivity (H_c). On the whole, the specimen with a Co-type precursor has the best comprehensive magnetic properties.

Author Contributions: Conceptualization, X.Z.; Resources, S.Z., J.L. and Y.Y.; Supervision, A.X.; Writing—original draft, X.Z. All authors have read and agreed to the published version of the manuscript.

Funding: This research received no external funding.

Institutional Review Board Statement: Not applicable.

Informed Consent Statement: Not applicable.

Conflicts of Interest: The authors declare no conflict of interest.

References

1. Sugimoto, M. The past, present, and future of ferrites. *J. Am. Ceram. Soc.* **1999**, *82*, 269–280. [[CrossRef](#)]
2. Pardavi-Horvath, M. Microwave applications of soft ferrites. *J. Magn. Magn. Mater.* **2000**, *215*, 171–183. [[CrossRef](#)]
3. Peng, L.; Li, L. Magnetic electrical and dielectric properties of microwave sintered $\text{Sr}_{1-x}\text{La}_x\text{Fe}_{12-x}\text{Ni}_x\text{O}_{19}$ ($x = 0-0.35$) hexaferrites used for nonreciprocal LTCF devices. *J. Mater. Sci. Mater. Electron.* **2017**, *28*, 17816–17826. [[CrossRef](#)]
4. Ogata, Y.; Kubota, Y.; Takami, T.; Tokunaga, M.; Shinokara, T. Improvements of magnetic properties of Sr ferrite magnets by substitutions of La and Co. *IEEE Trans. Magn.* **1999**, *35*, 3334–3336. [[CrossRef](#)]
5. Yang, Y.J.; Liu, X.S. Microstructure and magnetic properties of La-Cu doped M-type strontium ferrites prepared by ceramic process. *Mater. Technol.* **2014**, *29*, 232–236. [[CrossRef](#)]
6. You, L.S.; Qiao, L.; Zheng, J.W.; Jiang, M.Y.; Jiang, L.Q.; Sheng, J.W. Magnetic properties of La-Zn substituted Sr-hexaferrites by self-propagation high-temperature synthesis. *J. Rare Earths* **2008**, *26*, 81–84. [[CrossRef](#)]
7. Li, W.C.; Qiao, X.J.; Li, M.Y.; Liu, T.; Peng, H.X. La and Co substituted M-type barium ferrites processed by sol-gel combustion synthesis. *Mater. Res. Bull.* **2013**, *48*, 4449–4453. [[CrossRef](#)]

8. Liu, X.X.; Bai, J.M.; Wei, F.L.; Yang, Z. Magnetic and crystallographic properties of La-Zn substituted Sr-ferrite thin films. *J. Appl. Phys.* **2000**, *87*, 6875–6877. [[CrossRef](#)]
9. Teh, G.B.; Wong, Y.C.; Tilley, R.D. Effect of annealing temperature on the structural, photoluminescence and magnetic properties of sol-gel derived Magnetoplumbite-type (M-type) hexagonal strontium ferrite. *J. Magn. Magn. Mater.* **2011**, *323*, 2318–2322. [[CrossRef](#)]
10. Hessien, M.M.; Rashad, M.M.; El-Barawy, K. Controlling composition and magnetic properties of strontium hexaferrite synthesized by co-precipitation method. *J. Magn. Magn. Mater.* **2008**, *320*, 336–343. [[CrossRef](#)]
11. Rashad, M.M.; Ibrahim, I.A. A novel approach for synthesis of M-type hexaferrites nanopowders via the co-precipitation method. *J. Mater. Sci. Mater. Electron.* **2011**, *22*, 1796–1803. [[CrossRef](#)]
12. Tenaud, P.; Morel, A.; Kools, F.; le Breton, J.M.; Lechevallier, L. Recent improvement of hard ferrite permanent magnets based on La-Co substitution. *J. Alloys Compd.* **2004**, *370*, 331–334. [[CrossRef](#)]
13. Le Breton, J.M.; Teillet, J.; Wiesinger, G.; Morel, A.; Kools, F.; Tenaud, P. Mössbauer investigation of Sr-Fe-O hexaferrites with La-Co addition. *IEEE Trans. Magn.* **2002**, *38*, 2952–2954. [[CrossRef](#)]
14. Lechevallier, L.; Le Breton, J.M. Substitution effects in M-type hexaferrite powders investigated by Mössbauer spectrometry. *J. Magn. Magn. Mater.* **2005**, *290–291*, 1237–1239. [[CrossRef](#)]
15. Lechevallier, L.; Le Breton, J.M.; Morel, A.; Tenaud, P. On the solubility of rare earths in M-type SrFe₁₂O₁₉ hexaferrite compounds. *J. Phys. Condens. Matter* **2008**, *20*, 175203. [[CrossRef](#)]
16. Arabi, E.R.H.; Sarhaddi, R. Influence of nickel substitution on crystal structure and magnetic properties of strontium ferrite preparation via sol-gel auto combustion route. *Int. J. Mod. Phys. B* **2018**, *32*, 1750271.
17. Bai, J.M.; Liu, X.X.; Xie, T.; Wei, F.L.; Yang, Z. The effect of La-Zn substitution on the magnetic properties of Sr-magnetoplumbite ferrite nano-particels. *Mater. Sci. Eng. B* **2007**, *68*, 182–185. [[CrossRef](#)]
18. Qiao, L.; You, L.S.; Zheng, J.W.; Jiang, L.Q.; Sheng, J.W. The magnetic properties of strontium hexaferrites with La-Cu substitution prepared by SHS method. *J. Magn. Magn. Mater.* **2007**, *318*, 74–78. [[CrossRef](#)]
19. Yang, Y.; Wang, F.; Huang, D.; Shao, J.; Tang, J.; Rehman, K.M.U.; Wu, Z. Influence of Sn-Mg co-substitution on the microstructure and magnetic characteristics of M-type SrCaLa hexagonal ferrites. *J. Magn. Magn. Mater.* **2018**, *452*, 100–107. [[CrossRef](#)]